AIAA-82-0948
Vortex Simulation of an Inviscid Shear Layer

Y. Nakamura, A. Leonard and P. Spalart,
NASA Ames Research Center, Moffett Field, CA

AIAA/ASME 3rd Joint Thermophysics, Fluids, Plasma and Heat Transfer Conference
June 7-11, 1982/St. Louis, Missouri

VORTEX SIMULATION OF AN INVISCID SHEAR LAYER

A82-36253

Y. Nakamura,* A. Leonard,** and P. R. Spalart†
Ames Research Center, NASA, Moffett Field, California

Abstract

The accuracy of the vortex-blob method was tested by simulating a free-shear-layer instability, Kirchhoff's elliptical vortex, and a circular vortex. The main numerical parameters in the vortex-blob method are the density of the vortices, and the distribution of vorticity within each vortex core. The growth rate of a periodic unstable mode of the shear layer was calculated numerically and compared with the exact result. The error is only a few percent for about 10 rows of vortex blobs. The error is reduced by decreasing the spacing between vortices and, correspondingly, the core size. In the simulation of the motion of the elliptical vortex, the rotation of the boundary, without change of shape, and the circular particle paths of the vortical fluid were well simulated. For the circular vortex, optimum sets of parameters were obtained by comparing them with the exact velocity. The results are consistent with convergence theories of the vortex-blob method. In particular, second-order convergence is observed with a Gaussian core from velocity calculation.

I. Introduction

Recently the use of the vortex-blob method has received attention as a way to simulate two-dimensional, time-dependent, vorticity-dominated flows. In early applications of the vortex method to incompressible two-dimensional flows, point vortices were used. Although the point-vortex method yields exact solutions to the inviscid equations, it has the shortcoming that the vorticity and velocity fields are singular. The vortex-blob method was developed to avoid this shortcoming of the point-vortex method. In the vortex-blob method, the vorticity is distributed over "blobs" to remove the singularities. Leonard[1] reviewed these methods in detail, and Spalart and Leonard[2] have recently developed a new version of the blob method and applied it to flows past bluff bodies and airfoils.

The vortex-blob method produces vorticity distributions that are physically similar to those observed and that are more stable numerically. However, the method lacks the mathematical rigor of the point-vortex method. Hald and Del Prete[3] obtained rate of convergence $\delta^{3/4}$ when $\sigma = c_1\delta^{2/3}$, where σ denotes the core radius of the vortex blob and δ is the average distance between the vortices. They could prove convergence only for a small time interval. Subsequently, Hald[4] established the convergence of the vortex method for arbitrary long time intervals. He showed that if certain constraints on the vorticity profile of the vortex blob are satisfied then the L2 error in the position of vortices and the L2 error in the computed velocity field are both of the order of δ^2, and the L2 error in the vorticity distribution is of the order of $\delta^{3/2}$ if $\sigma = c_2\delta$. Hald also showed that the method converges quadratically, even with $\sigma = c_3\delta^{1/2}$. Subsequently, Beale and Majda[5,6] derived an improved proof of convergence, showing that vortex-blob methods of arbitrarily high-order accuracy are possible, using the vorticity profiles discussed in Ref. 1. They also generalized and simplified the earlier stability proof due to Hald.[4]

Obviously, the consistency and the accuracy of the vortex-blob method depend on a proper choice of the parameters. The parameters considered in this paper are distance between the vortices, the core size, the velocity scheme by which each vortex is moved, and the core shape. These parameters are described in detail by Leonard.[1] In this paper, we report the results of test problems used to study the accuracy of the vortex-blob method. The method was applied to the following three problems: a free shear layer, Kirchhoff's elliptic vortex, and a circular vortex.

In the free-shear-layer problem, the growth rate of a small disturbance was observed as a result of simulation of the free shear layer. The results were compared with analytical results which were obtained by solving the Rayleigh equation.[7]

In the second problem, the vortex blob method was applied to simulate the motion of Kirchhoff's elliptical vortex. The exact solution is known,[1] and the elliptic vortex should rotate without change of shape. Furthermore, each particle path within the elliptic vortex is circular. For the circular vortex problem, the L2 error in the velocity field is calculated to obtain relations between the error, the core radius, and the distance between the vortices. The fourth-order Runge-Kutta scheme was used for time-integration throughout these calculations. The errors that result from the time-step size in both the Euler and Runge-Kutta schemes are described for Kirchhoff's elliptical vortex. These errors may be related to an effective viscosity, because the effective viscosity is calculated from the time derivative of a double integration of the second moment of vorticity.

II. Parameters of the Method

In the following studies two core shapes (i.e., vorticity distribution within each vortex core) were used: Gaussian and spectral (see Ref. 1). These distributions are defined as follows.

Gaussian core:

$$g(|x - x_j|/\sigma) = 1 - \exp(-|x - x_j|^2/\sigma^2) \qquad (1)$$

Spectral core:

$$g(|x - x_j|/\sigma) = 1 - J_0(2|x - x_j|/\sigma) \qquad (2)$$

where $g(y)$ is the circulation at radius y, and is equal to

$$g(y) = 2\pi \int_0^y f(z) z \, dz \qquad (3)$$

*NRC Research Associate. Member AIAA.
**Research Scientist. Member AIAA.
†Research Assistant, Stanford University, Palo Alto, Calif. Member AIM.

where $f(z)$ is the vorticity distribution within the blob.

We also test two assumptions concerning the velocity of each blob: scheme A, in which the velocity field is evaluated at the center of the blob, and scheme B, in which the vorticity-weighted average of the velocity field over the blob is used. Scheme B requires more computational effort but conserves energy.[1] The blob velocities are given by the following.

Scheme A:

$$\frac{d\mathbf{x}_i}{dt} = \mathbf{u}(\mathbf{x}_i,t) = -\frac{1}{2\pi}\sum_{j=1}^{N}\frac{(\mathbf{x}_i-\mathbf{x}_j)\times\hat{e}_z\Gamma_j g(|\mathbf{x}_i-\mathbf{x}_j|/\sigma_j)}{|\mathbf{x}_i-\mathbf{x}_j|^2} \tag{4}$$

Scheme B:

$$\frac{d\mathbf{x}_i}{dx} = \int\gamma_i(\mathbf{x}_i-\mathbf{x}')\mathbf{u}(\mathbf{x}',t)d\mathbf{x}' = -\frac{1}{2\pi}\sum_{j=1}^{N}\frac{(\mathbf{x}_i-\mathbf{x}_j)\times\hat{e}_z\Gamma_j m(|\mathbf{x}_i-\mathbf{x}_j|,\sigma_i,\sigma_j)}{|\mathbf{x}_i-\mathbf{x}_j|^2} \tag{5}$$

where Γ_j is the strength of circulation of jth blob, and

$$m(|\mathbf{x}_i-\mathbf{x}_j|,\sigma_i,\sigma_j) = (2\pi)^2\int_0^\infty\int_0^\infty xy\, f(\mathbf{x})\, f(y)q(|\mathbf{x}_i-\mathbf{x}_j|,\sigma_i x,\sigma_j y)dx\,dy \tag{6}$$

and

$$q(z,s,t) = \begin{cases} 1 & s+t \leq z \\ \frac{1}{\pi}\cos^{-1}\frac{s^2+t^2-z^2}{2st} & |s-t| \leq z \leq s+t \\ 0 & z \leq |s-t| \end{cases} \tag{7}$$

In this paper, the m function in scheme B has been replaced by a cubic spline approximation. Calculations using scheme B were carried out with Gaussian cores only. The effective circulation distributions for three major types are depicted in Fig. 1 for the case of $\sigma = 0.4$. The spectral core oscillates into the far field. The distribution of scheme B with a Gaussian core is similar to that of scheme A with a larger core. In addition to the parameters discussed above, the effect on the accuracy of the results of core size and of the average distance between vortices was examined.

III. Free Shear Layer

Two-dimensional inviscid free-shear-layer instabilities were simulated for three base-flow distributions U(y): hyperbolic tangent, error function, and polynomial. These velocities are expressed as follows.

Hyperbolic tangent:

$$U(y) = 0.5(1 + \tanh y) \tag{8}$$

Error function:

$$U(y) = \frac{1}{\tilde{\sigma}(\pi)^{1/2}}\int_0^y \exp(-y^2/\tilde{\sigma}^2)dy + 0.5 \tag{9}$$

where $\tilde{\sigma} = 1.128$.

Polynomial:

$$U(y) = \begin{cases} 1 & Y > 1/h \\ -hy[0.5(hy)^3 - (hy)^2 + 1] + 0.5 & 1/11 > y > 0 \\ hy[-0.5(hy)^3 - (hy)^2 + 1] + 0.5 & 0 > y > -1/h \\ 0 & -1/h > y \end{cases} \tag{10}$$

where $h = 0.5$. In each case, $U(\infty) = 1$, $U(-\infty) = 0$, and $dU/dy|_{y=0} = 0.5$. In the fourth-order polynomial base flow the vorticity is confined to $|y| \leq 2$. The velocity and vorticity distributions are shown in Fig. 2. The hyperbolic-tangent base flow was investigated, initially, because its growth rate had already been obtained by Michalke.[7] However, as seen in Fig. 2, the vorticity distribution in the hyperbolic-tangent base flow does not decay rapidly for large $|y|$. In order to reduce the domain to be covered by the vortex blobs and to investigate the effect of the base-flow profile, the cubic function and Gaussian vorticity distributions were also considered.

Finally, the effect of the average distance between vortices was examined by varying the number of rows of vortex blobs from 7 to 11. For this first problem, only scheme A with Gaussian cores was implemented.

Base Flow

In order to obtain accurate growth rates, the base flow must be represented in terms of the blobs as precisely as possible. Therefore, we calculated the circulation for each vortex row, using a least-squares method. The quantity to be minimized is

$$H = \int_{-\infty}^{\infty}\left\{\Omega(y) - \sum_i \Gamma_i[\psi(y-y_i) + \psi(y+y_i)]\right\}^2 dy + \lambda\left(\sum_i \Gamma_i - 0.5\right) \tag{11}$$

where $\Omega(y)$ is the exact vorticity distribution function. For each i, one row of strength Γ_i is placed on each side of the axis. The second term on the right-hand side represents the constraint on total circulation, and the λ is the Lagrange multiplier. The function ψ is the average of the blob distribution over the x-direction. When

$$\psi = \frac{1}{(\pi)^{1/2}\sigma_i}\exp[-(y-y_i)^2/\sigma_i^2] \tag{12}$$

minimizing H with respect to Γ_i and λ yields the simultaneous equations for Γ_k and λ.

$$2 \sum_i \int_{-\infty}^{\infty} [\psi(y - y_i) + \psi(y + y_i)][\psi(y - y_k) + \psi(y + y_k)]dy\Gamma_k + \lambda = 2 \int_{-\infty}^{\infty} \Omega(y)[\psi(y - y_k) + \psi(y + y_k)]dy \qquad k = 1,2, \ldots \quad (13)$$

and

$$\sum_i \Gamma_i = 0.5 \quad (14)$$

The results for the errors of each of these best approximations are shown in Fig. 3.

The error-function base flow is approximated with a much smaller minimum error than is the hyperbolic-tangent base flow for the same core size, σ. On the other hand, the polynomial base flow requires smaller σ than the other base flows because of the small extent of the shear layer for the polynomial case. However, when $\sigma \geq 0.3$ (in particular for this base flow), we obtain oscillatory, positive and negative values for the sequence of circulations, Γ_i, for some vortex spacings, δ. Although larger values of σ produced smaller errors in representing the hyperbolic-tangent and error-function base flows within the limits examined here, the polynomial base flow results suggest that if σ is too large, undesirable oscillatory values for Γ_i may be obtained, and, therefore, there is an optimum value of the core radius, σ, to be used in representing the base flow.

In each base flow, if δ is too small, the error increases and also leads to oscillation of the Γ_i. Therefore, there is also an optimum value of the distance between vortices for a fixed number of blob rows. The minimum error at this optimum value of δ can be reduced by increasing the number of blob rows, as can be seen from Fig. 3 by observing the effect of the number of rows.

However, these optimum values with minimum errors in the base-flow representation do not necessarily represent the inviscid fluid dynamics with minimum error. As described later, the error in the dynamics generally increases with increasing initial vortex spacing.

The errors might have to be made dimensionless for comparison by dividing them by

$$\int_{-\infty}^{\infty} \Omega^2 \, dy \quad (15)$$

which is the integral of the square of the base-flow vorticity. The square root of this quantity for the hyperbolic-tangent, error-function, and polynomial base flows, respectively, is 0.5774, 0.5946, and 0.6095. Anyway, the absolute errors were used here.

Dependence on the x-Direction

The x- and y-distances between the vortices Δx and Δy, were equal throughout the shear-layer simulation. For the x-direction, periodical boundary conditions were used: the velocity field has contributions from every vortex in the periodic x-domain and from all the periodic images of these vortices. Since the Gaussian vorticity distribution decays sufficiently rapidly, it is assumed that g is unity for all periodic images except for the nearest one, which were treated as point vortices. Consequently,

$$u = \frac{1}{2\pi} \frac{y - y_j}{r^2} \Gamma_j \exp(-r^2/\sigma^2) - \frac{\Gamma_j}{2L} \frac{\sinh[2\pi(y - y_j)/L]}{\cosh[2\pi(y - y_j)/L] - \cos[2\pi(x - x_j)/L]} \quad (16)$$

$$v = -\frac{1}{2\pi} \frac{x - x_j}{r^2} \Gamma_j \exp(-r^2/\sigma^2) + \frac{\Gamma_j}{2L} \frac{\sin[2\pi(x - x_j)/L]}{\cosh[2\pi(y - y_j)/L] - \cos[2\pi(x - x_j)/L]} \quad (17)$$

where L is the wavelength.

Example of Large Deformation Growth

The time evolution of the instability of the free shear layer is shown for an error-function base flow with $\Delta x = \Delta y = 0.5$ (Fig. 4). The total number of vortices used was 336 (7 rows, 48 vortices in each row). The initial perturbation strength was $\varepsilon = 0.01$ (defined below), and the number of steps calculated was 100. In this case, the uniform velocity of -0.5 was added to simplify observation of the pattern of change. With time, the disturbance grows, producing the well-known vortex formation.

Growth of a Small Perturbation

Our concern, however, is with the early stage of instability growth, which is nearly linear, because we have the exact result.[7] Therefore, the vortex-blob method was applied to this instability problem with a very small initial perturbation strength, $\varepsilon = 0.00001$.

Michalke[7] applied the Rayleigh equation to small perturbations of a hyperbolic-tangent base flow and developed a method to compute the growth rate as an eigenvalue. The same method has been applied here to the other two base flows considered. These results are shown in Fig. 5. Note that as θ, the momentum thickness of the base flow, decreases ($\theta_h = 0.5$, $\theta_e = 0.4502$, $\theta_p = 0.2087$), the corresponding maximum wave number of instability decreases ($\alpha_h = 1.0$, $\alpha_e = 0.92$, $\alpha_p = 0.874$).

To measure the growth of the disturbance, in the numerical simulation, we calculate

$$F(\alpha,t) = \left[\int_{-\infty}^{\infty} \left| \int_{-L/2}^{L/2} e^{i\alpha x} \omega(x,y,t)dx \right|^2 dy \right]^{1/2} \quad (18)$$

at each time-step, where a is the disturbance wave number. For the Gaussian core, we find

$$F(\alpha,t) = \left\{ \sum_{j=1}^{N} \frac{\Gamma_i^2}{(2\pi)^{1/2}\sigma_i L^2} \exp -\left(\frac{\alpha^2\sigma_i^2}{2}\right) + \sum_{i>j}\sum \frac{(2)^{1/2}\Gamma_i\Gamma_j}{(\pi)^{1/2}\sigma_i L^2} \exp\left(-\frac{\alpha^2\sigma_i^2}{2}\right) \times \exp\left[-\frac{(y_i - y_j)^2}{2\sigma_i^2}\right] \cos k(x_i - x_j) \right\}^{1/2} \quad (19)$$

Using this relation, the growth rate was obtained as the ratio of values at the nth and (n + 1)th steps as follows:

$$\alpha c_i \Big|_n^{n+1} = \log[F(\alpha,t)^{n+1}/F(\alpha,t)^n] \quad (20)$$

This should be divided by the time-step size to get the actual growth rate.

Initial Perturbation

The analytical form of the perturbation vorticity is given by

$$\Delta\omega = e^{ac_i t}[\omega_r(y)\cos\alpha(x - c_r t) - \omega_i(y)\sin\alpha(x - c_r t)] \quad (21)$$

where ω_r and ω_i are real and imaginary parts of the perturbed vorticity. These were calculated by Michalke's method. Each vortex blob was assigned a strength corresponding to the initial perturbed vorticity distribution given by

$$\Omega_t = \Omega(y) + \varepsilon[\omega_r(y)\cos ax - \omega_i(y)\sin ax] \quad (22)$$

where $\Omega(y)$ was determined from the base-flow simulation. The value of ε was 0.00001. Two remarks are in order. First, changing ε by a factor of 10 did not change the growth rate, which shows that the disturbance was in the linear range. Secondly, although information from linearized theory was used in Eq. (21), the constancy of the growth rate with time shows that the most unstable numerical mode is already dominant.

Simulated Results

In the present simulation, the wavelength L was set equal to 24. Consequently, the wave number $\alpha = 2\pi/L$ is equal to 0.2618. Analytical growth rates for this value of a are 0.0813 €or the hyperbolic-tangent base flow; 0.0828 for the error-function base flow; and 0.0838 for the polynomial base flow. Fourth-order Runge-Kutta time integration was used with $\Delta t = 0.5$. Preliminary calculations showed this value of Δt to be the maximum time-step allowable for the hyperbolic-tangent base flow having negligible time-differencing error at t = 2. Forty steps were calculated. The computed growth rates versus time are shown in Fig. 6.

The parameters used in these calculations are shown in each figure. The average distance between vortices 6 was determined in such a way that the x-direction spacing of vortex blobs has figures that are as simple as possible. The core size of the vortex blob a was chosen arbitrarily, but to satisfy the requirement that $\beta < 1$ in $a = c_3\delta^\beta$; this is defined below. Generally, the polynomial base-flow results were nearest the exact growth rate and those of the hyperbolic-tangent base flow were farthest from it. In the three base flows, the runs with large 6 resulted in growth-rate oscillation. All growth rates were less than about 9% at about t = 20. As 6 becomes smaller, the accuracy improves. The results shown in Fig. 6 can be used to estimate convergence rates. The results are shown in Fig. 7, where each last growth rate was used as a representative value. Relations between ε (error), σ, and 6 of the type $\varepsilon = c_1\delta^\gamma$, $\varepsilon = c_2\sigma^p$, and $a = c_3\delta^\beta$ were calculated from these data, using a least-squares method. These results are shown in Table 1. The polynomial-base flow had the best convergence rate in terms of 6, and the hyperbolic-tangent base flow had the worst. It is plausible that the convergence rates for 6 were less than 2 but not very much so, except for the hyperbolic-tangent base flow. As shown in the second problem, the Gaussian core seems to have nearly second-order convergence for σ. The reason the hyperbolic-tangent base flow had a convergence rate that is greater than 2 for a might be an unfavorable choice of a.

IV. Kirchhoff's Elliptic Vortex

The vortex-blob method was used to compute the motion of Kirchhoff's elliptic vortex, an elliptical region of constant vorticity. Zabusky et al.[9] simulated this flow by using the contour dynamics method, in which computational points are required only along the boundary of the ellipse. This problem has an exact solution in which the overall elliptic vortex rotates without change of shape.' The angular velocity of the ellipse is

$$n = \frac{ab\omega}{(a + b)^2} \quad (23)$$

where a and b denote the major and minor semiaxes of the ellipse, and ω is the value of the vorticity. Since a = 4, b = 3, and $\omega = 400/(\pi ab) = 10.61$ in this paper, n = 2.598 sec^{-1}. Another interesting feature of this flow is that the particle paths within the vortex are circles and the angular velocity around the circle is twice (2n) that of the ellipse.

To simulate this elliptical-vortex flow. vortex blobs were distributed on concentric ellipses ac equal eccentric angles along each ellipse. The number of blobs for each ellipse was determined in such a way that each blob occupied the same area; that is,

$$M = A(2n - 1) \quad (24)$$

for the nth elliptical ring, and A was set to 4.

The overall rotation of the ellipse without change of shape was well simulated, as shown in Fig. 8. Scheme A was used with Gaussian cores with σ = 0.4 and eight rings.

To obtain a quantitative measure of the rotation, the (x,y) correlation of the vortex locations was computed. This was defined by

$$\rho_{xy} = \frac{\frac{1}{N}\sum_i (x_i - \bar{x})(y_i - \bar{y})}{\left[\frac{1}{N}\sum (x_i - \bar{x})^2 \frac{1}{N}\sum (y_i - \bar{y})^2\right]^{1/2}} \qquad (25)$$

where

$$\bar{x} = \frac{1}{N}\sum x_i , \qquad \bar{y} = \frac{1}{N}\sum y_i \qquad (26)$$

The exact value for this correlation taken over all material points in a rotating ellipse is given by

$$\rho_{xy}^{exact} = \frac{a^2 - b^2}{2ab} \sin(2nt) \qquad (27)$$

One computed example is shown together with the exact result in Fig. 9. The calculated rotation period is 2.418. The deviation from the exact value is less than 0.05%. In the simulation, 10 rings with Gaussian cores with $\sigma = 0.3$ and scheme A were used.

In Fig. 10, the difference between the trajectory of a particle and the exact circle are shown for scheme A, scheme B, and for the spectral core. The exact particle path is expressed by

$$\left.\begin{aligned} x' &= A\cos(2nt + \phi) + B\cos\phi \\ y' &= A\sin(2nt + \phi) + B\sin\phi \end{aligned}\right\} \qquad (28)$$

where $A = k(a + b)/2$ and $B = k(a - b)/2$. In this calculation $k = 0.9375$ and $\phi = 0$, since the trajectory of a vortex particle with the maximum value of x at the initial time was sought, that is, with $x = 3.75$ and $y = 0$. The calculation was done with eight rings and $a = 0.4$. The dashed lines show the exact circle trajectories. In Fig. 10b, the time history of the radius from the exact center of the circle is shown for each case. In this comparison it is seen that the spectral core produces superior results for $\sigma = 0.4$. It appears that the spectral core is effective for rather large core radii.

To separate the spatial error from the time-integration errors, the minimum error in the initial vortex velocities is depicted for scheme A in Fig. 11 as a function of average distance between the vortices calculated as the square root of the area each vortex occupies. The following expression for velocity error ε was used:

$$\varepsilon = \left[\frac{\sum_{j=1}^{J}\left(\sum_{i=1}^{N} u_i - u_e\right)^2 + \left(\sum_{i=1}^{N} v_i - v_e\right)^2}{J}\right]^{1/2} \qquad (29)$$

where N denotes the total number of vortices, and u_e and v_e are the exact velocities,

$$u_e = -n\frac{a+b}{b}y , \qquad v = n\frac{a+b}{a}x \qquad (30)$$

inside the elliptical vortex. The maximum exact velocity is 18.19 from $ab\omega/(a + b)$, which occurs at the perimeter of the ellipse. The velocities were calculated at grid points with the mesh of 31×31 in $0 \leq x \leq 4$ and $0 \leq y \leq 3$, but within the ellipse.

The actual convergence of the vortex-blob method for this problem depends on the relations between ε, σ, and δ. In particular, δ should tend to zero faster than σ. A one-dimensional interpretation for this constraint is provided in the Appendix. Those relations were calculated from the vortex velocity. The optimum core radius was determined to minimize the error.

Gaussian core:

$$\varepsilon \sim \delta^{1.35} \quad \text{with} \quad \sigma \sim \delta^{0.934} \qquad (31)$$

Spectral core:

$$\varepsilon \sim \delta^{1.54} \quad \text{with} \quad \sigma \sim \delta^{1.02} \qquad (32)$$

The reason convergence is not as fast for the core radius as for the expected relations $\varepsilon \sim \sigma^2$, might be a result of the step present in the vorticity distribution. Furthermore, the present method of distributing the vortex blobs on the ellipse might not give the best results.

To confirm this conjecture, the same error was calculated for the circular vortex, with the vorticity distribution given by the cubic function defined by $\omega = 1 - 3r^2 + 2r^3 (0 \leq r \leq 1)$ and $\omega = 0$ for $r > 1$. Thus, ω is a smooth function. The results are shown in Fig. 12, where the following relations were found.

Gaussian core:

$$\varepsilon \sim \delta^{1.75} \quad \text{with} \quad \sigma \sim \delta^{0.875} \qquad (33)$$

Spectral core:

$$\varepsilon \sim \delta^{1.59} \qquad (34)$$

We observe exactly second-order convergence in terms of a for the Gaussian core, as expected. With the spectral core, the error was rather insensitive to core radius, and smaller than with the Gaussian core.

Finally, the effect of the time-integration errors for both the Euler scheme and Kunge-Kutta scheme was examined by calculating the effective viscosity. Theoretically, the time derivative of the second moment of the vorticity is proportional to the viscosity:"

$$\frac{d}{dt}\iint \omega r^2 \, dx\, dy = \nu \iint \omega \, dx\, dy \qquad (35)$$

If the fluid is nonviscous, the left-hand-side term should be equal to zero. In actuality, however, because of the effect of the time-integration scheme, this term does not vanish. This error was estimated by calculating the effective viscosity derived from Eq. (35) as follows:

$$\nu_{eff} = \frac{\frac{d}{dt}\left(\sum_i \Gamma_i r_i^2\right)}{\sum_i \Gamma_i} \qquad (36)$$

The time derivative in the numerator is estimated as the difference between the values at the first and second step. The result is shown in Fig. 13, where eight rings and scheme A with $\sigma = 0.3$ were used. By a least-squares method, the following relationships were found.

Euler method:

$$\nu_{eff} \sim (\Delta t)^{0.979} \tag{37}$$

Runge-Kutta method:

$$\nu_{eff} \sim (\Delta t)^{5.17} \tag{38}$$

This is consistent with theory, since the fourth-order Runge-Kutta scheme is fifth-order accurate in amplitude when the eigenvalues are imaginary; the Euler scheme is of first order. The effective viscosity tends to zero with the time-step, which shows that no diffusion is associated with the spatial errors. The vortex method is "semi-inviscid."

V. Summary

1) The accuracy of the vortex-blob method was investigated by applying the method to three different problems: the instability of a free shear layer, the motion of Kirchhoff's elliptic vortex, and the motion of a circular vortex.

2) In base-flow simulation of the free shear layer, there is an optimum value for δ, the distance between the vortices, because of the limited number of rows of the blob. Furthermore, an optimum value exists also for σ, the core size. However, these relations do not necessarily represent the inviscid fluid dynamics with minimum error, since the results of the dynamic equation show that the smaller distance has a better accuracy.

3) In shear-layer simulations, we had the following relations between ε, a, and δ: $\varepsilon \sim \delta^{1.30}$ when $\sigma \sim \delta^{0.571}$ for the hyperbolic-tangent base flow; $\varepsilon \sim \delta^{1.47}$ when $\sigma \sim \delta^{0.768}$ for the error-function base flow; and $\varepsilon \sim \delta^{1.85}$ when $\sigma \sim \delta^{0.922}$ for the polynomial base flow. The convergence is roughly of second order in terms of σ.

4) In Kirchhoff's elliptic vortex, the overall rotation without change of shape was generally well simulated by the vortex-blob method. The calculated x-y correlation was almost the same as the theoretical value. In addition to these things, the representative particle path was simulated. In this case, the spectral core showed the best fit, and scheme B the worst. In all cases, the deviation from the exact radius grew with time.

5) Generally, the smaller the distance δ becomes, the smaller the error becomes. Of course, as δ is decreased, the core size σ must decrease. From the calculation of the initial velocity of the elliptic vortex, the following relations were obtained: $\varepsilon \sim \delta^{1.35}$ with $\sigma \sim \delta^{0.934}$ for the Gaussian core, and $\varepsilon \sim \delta^{1.54}$ with $\sigma \sim \delta^{1.02}$ for the spectral core. The error is not very small, because the exact elliptic vortex has step functions in the vorticity distribution, which makes it difficult to fit the velocity.

6) The relations between ε, σ, and δ were also calculated with the circular vortex, which has the cubic function vorticity distribution, a smoother distribution than that of the elliptic vortex. As a result, the following relations were obtained: $\varepsilon \sim \delta^{1.75}$ with $\sigma \sim \delta^{0.875}$ for the Gaussian core, and $\varepsilon \sim \delta^{1.59}$ for the spectral core. In the case of the Gaussian core, the convergence rate was second order in σ as was expected. The spectral core was insensitive to core radius.

7) In Kirchhoff's elliptic vortex simulation, the Runge-Kutta scheme showed fifth-order convergence in terms of time-step, using an effective viscosity criterion, and the Euler method showed first-order convergence. These convergences agree with the theoretical interpretation.

Appendix: On the Relation between σ and δ

It can be shown on a simple one-dimensional model why the core size σ should not tend to zero as fast as the average distance between vortices, δ. This is necessary for the initial distribution of the vorticity to properly approximate the exact initial distribution. The accuracy of the dynamics at later times depends on the accuracy of the initialization.

Let us consider a given function F defined on $-\infty, +\infty$; F is supposed to be smooth and to be in L2. Let $\hat{F}$ be its Fourier transform. An approximation to F is given by

$$F_{\delta,\sigma}(x) = \sum_{n=-\infty}^{\infty} A^n_{\delta,\sigma} g\left(\frac{x - n\delta}{\sigma}\right) \tag{A1}$$

The approximation $F_{\delta,\sigma}$ is made up of "blobs" of a given shape g (for instance, Gaussian), of size a, and spaced by δ, in the same way as is done in the vortex-blob method. As δ and σ both tend to zero, $F_{\delta,\sigma}$ is supposed to converge to F.

The Fourier transform of $F_{\delta,\sigma}$ is:

$$F_{\delta,\sigma}(\alpha) \quad \sum_{n=-\infty} A^n_{\delta,} \quad \exp(i\alpha n\delta/\sigma)\sigma\hat{g}(\alpha\sigma)$$

The value of at $\alpha = 2\pi/\delta$ is:

$$F_{\delta,\sigma}(2\pi/\delta) = \sum_{n=-\infty}^{\infty} \sigma A^n_{\delta,\sigma}\, \hat{g}(2\pi\sigma/\delta) \tag{A3}$$

The first factor can be written as

$$\sum_{n=-\infty}^{m} \sigma A^n_{\delta,\sigma} = \frac{\int_{-\infty}^{\infty} F_{\delta,\sigma}(x)\,dx}{\int_{-\alpha}^{\infty} g(x)\,dx} \tag{A4}$$

As $F_{\delta,\sigma}$ converges to F, the integral of $F_{\delta,\sigma}$ tends to the integral of F, which is not generally zero. The integral of g is also a constant. Therefore, $\hat{F}_{\delta,\sigma}(2\pi/\delta)$ is of the same order as $\hat{g}(2\pi\sigma/\delta)$, when δ and σ tend to zero. Now, since F is smooth, $\hat{F}(2\pi/\delta)$ tends to zero as $2\pi/\delta$

tends to infinity; therefore, $\hat{F}_{\delta,\sigma}(2\pi/\delta)$ should tend to zero also. This is not possible if σ/δ is held constant; in general (in particular if g is Gaussian) σ/δ will have to tend to infinity as δ tends to zero. In other words, σ tends to zero more slowly than δ, and the blobs will overlap more and more as δ tends to zero. Otherwise, there is an error of period δ (wave number $2\pi/\delta$) with an amplitude that does not tend to zero. This interpretation is consistent with Hald's method; Hald takes $\sigma = \delta^{\beta}$, with $\beta < 1$.

References

[1]Leonard, A., "Vortex Methods for Flow Simulation," Journal of Computational Physics, Vol. 37, 1980, pp. 289–335.

[2]Spalart, P. R. and Leonard, A., "Computation of Separated Flows by a Vortex-Tracing Algorithm'," AIAA Paper 81–1246, Palo Alto, Calif., 1981.

[3]Hald, O. H. and Del Prete, V. M., "Convergence of Vortex Methods for Euler's Equations," Mathematics of Computation, Vol. 32, 1978, pp. 791–809.

[4]Hald, O. H., "Convergence of ,Vortex Methods for Euler Equations. II, SIAM Journal on Numerical Analysis, Vol. 16, 1979, pp. 726–755.

[5]Beale, J. T. and Majda, A., "The Design and Numerical Analysis of Vortex Methods," *PAM–48*, Center for Pure and Applied Mathematics, University of California, Berkeley, Calif., 1981.

[6]Beale, J. T. and Majda, A., "Vortex Methods, II: Higher Order Accuracy in Two and Three Dimensions," PAM–54, Center for Pure and Applied Mathematics, University of California, Berkeley, Calif., 1981.

[7]Michalke, A., "On the Inviscid Instability of the Hyperbolic-Tangent Velocity Profile," Journal of Fluid Mechanics, Vol. 19, 1964, pp. 543–556.

[8]Lamb, H., Hydrodynamics, 6th ed., Dover, New York, 1932.

[9]Zabusky, N. J., Hughes, M. H. and Roberts, K. V., "Contour Dynamics for the Euler Equations in Two Dimensions," Journal of Computational Physics, Vol. 30, 1979, pp. 96–106.

[10]Ting, L., "Integral Invariants and Decay Laws of Vorticity Distributions," Bulletin of the American Physical Society, Vol. 26, 1981, pp. 1273–1274.

Table 1 Exponents for relations between error, core radius, and distances between vortices: $\varepsilon = c_1\delta^{\gamma}$, $\varepsilon = c_2\sigma^{p}$, and $\sigma = c_3\delta^{\beta}$

Base flows	Exponent		
	p	β	2
Hyperbolic tangent	2.27	0.571	1.30
Error function	1.92	0.768	1.47
Polynomial	2.01	0.922	1.85

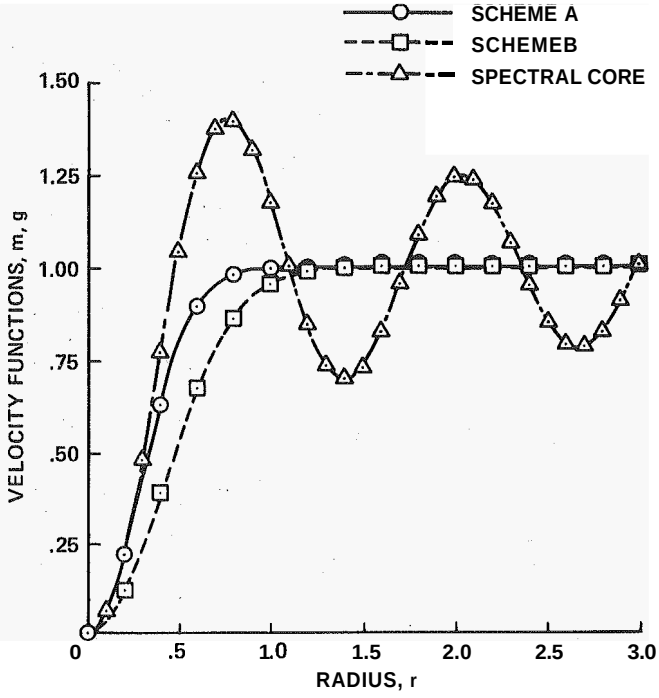

Fig. 1 Induced velocity functions m and g as a function of radius: $\sigma = 0.4$.

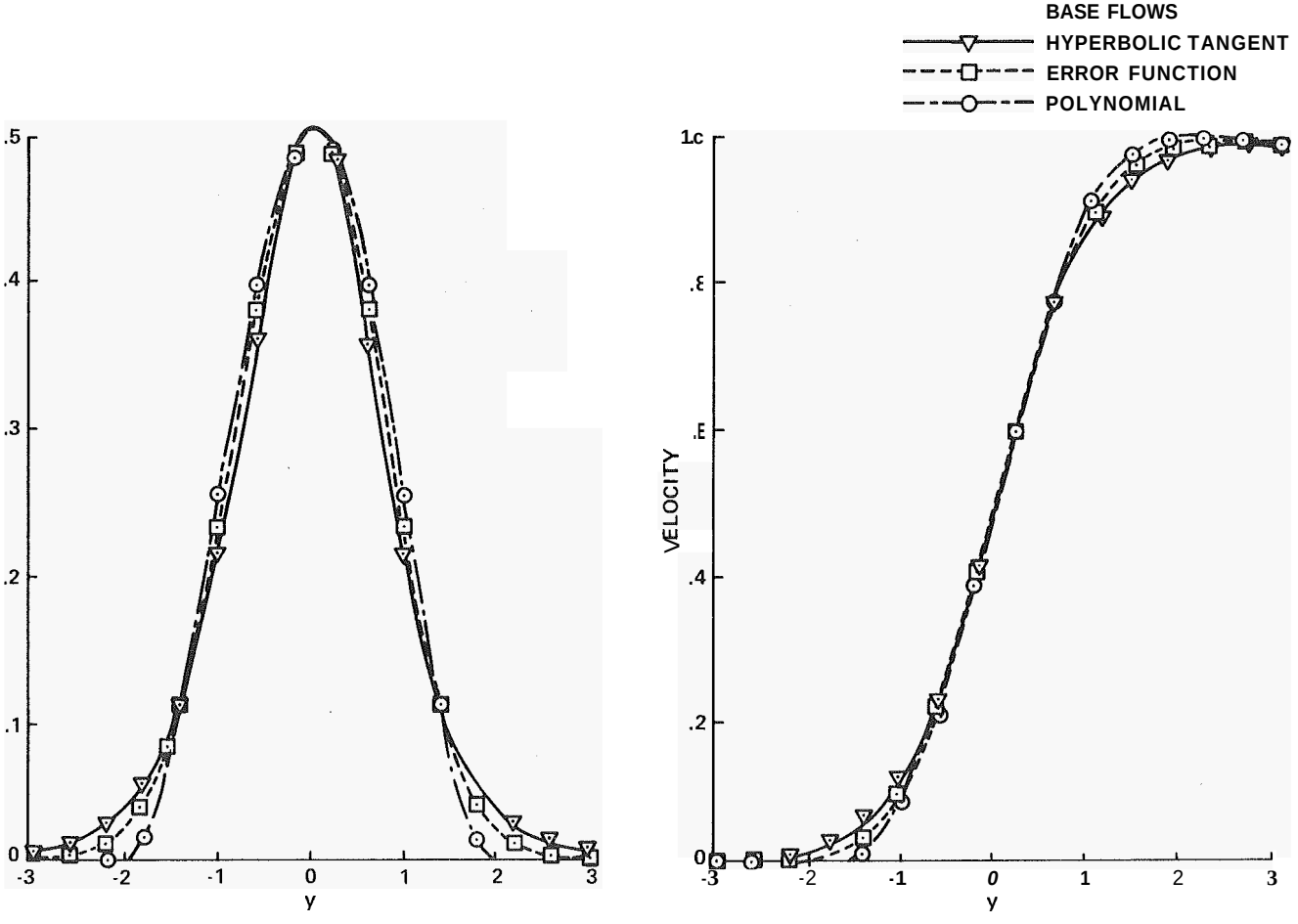

a) Vorticity distribution

b) Velocity distribution

Fig. 2 Base flows for the free shear layer.

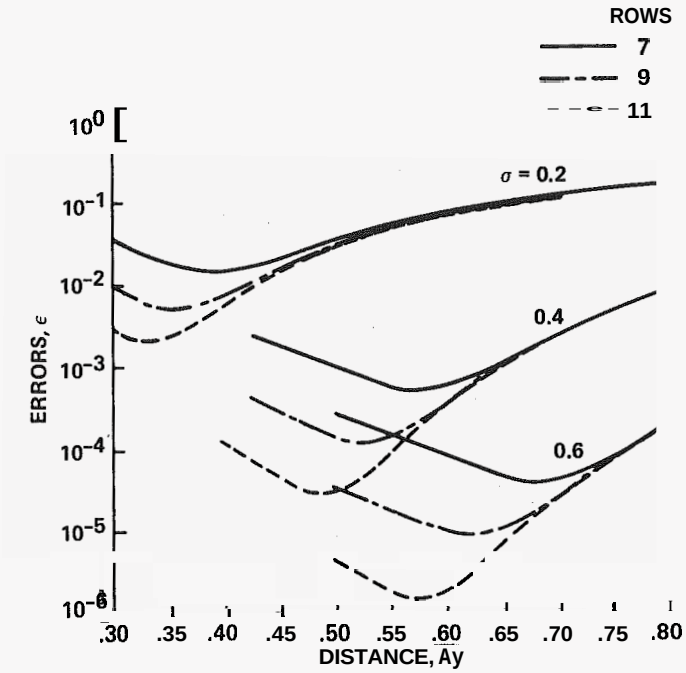

a) Hyperbolic-tangent base flows

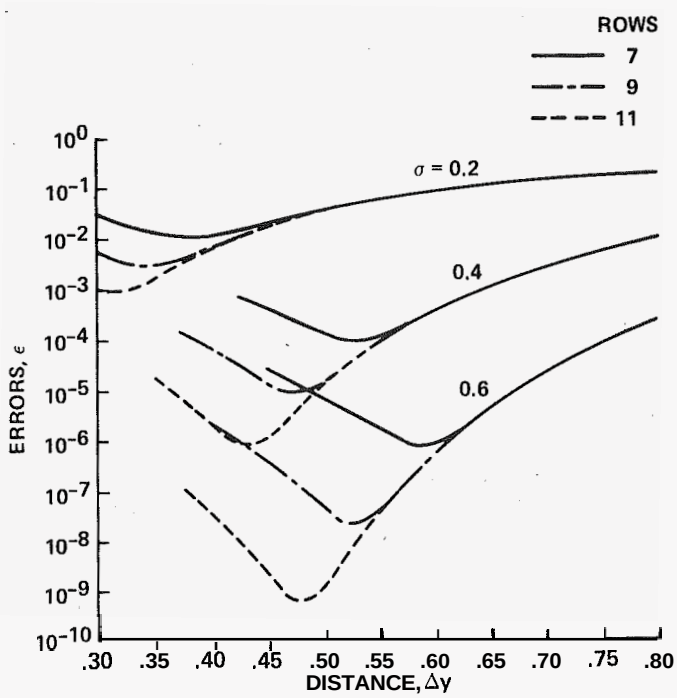

b) Error-function base flows

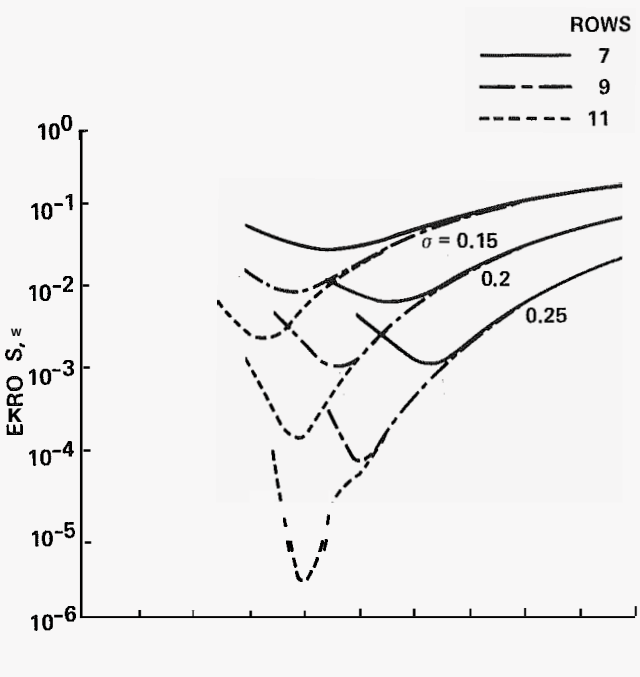

c) Polynomial base flows

Fig. 3 Error in base-flow representation by vortex-blob method.

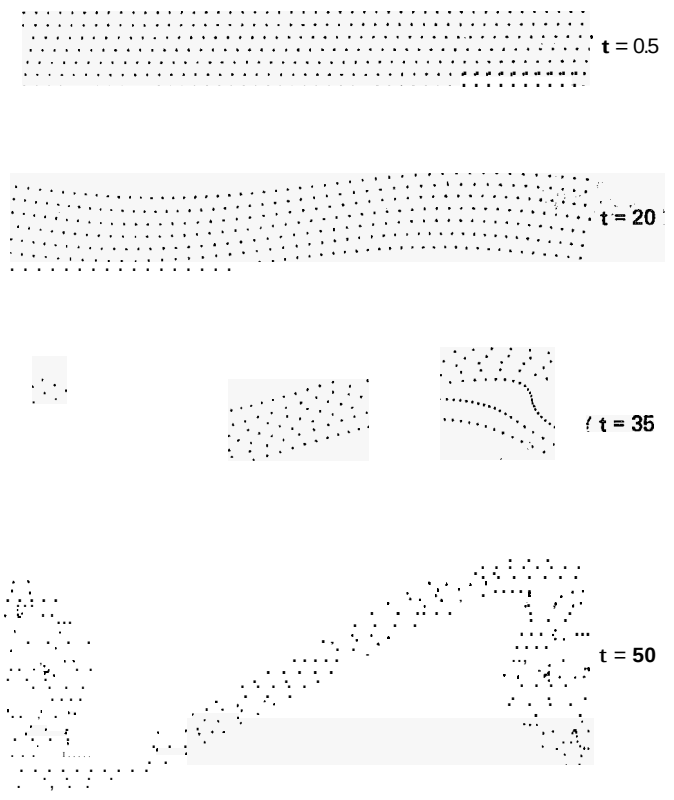

Fig. 4 Evolution of a free-shear-layer instability — error-function base flow: $\delta = 0.5$, $\sigma = 0.4$, $\varepsilon = 0.01$.

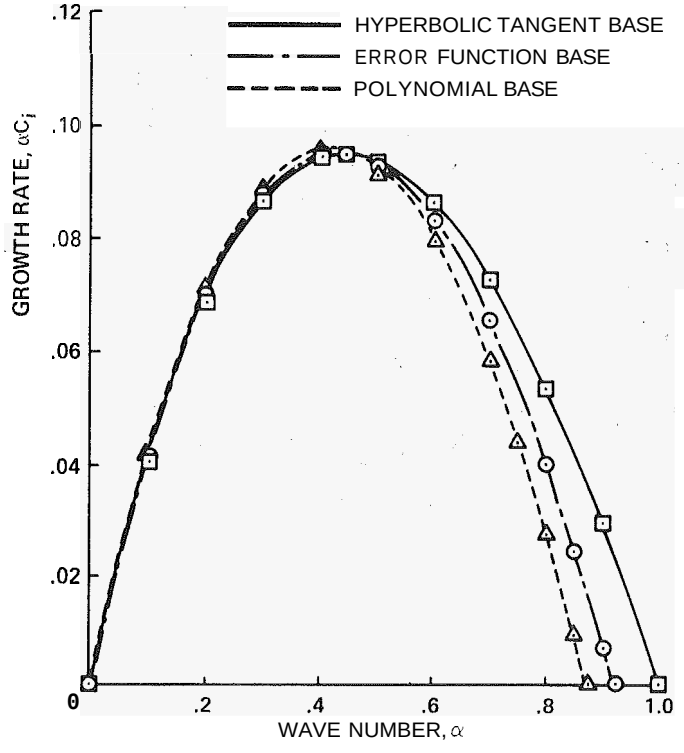

Fig. 5 Analytical growth rates of a free-shear-layer instability.

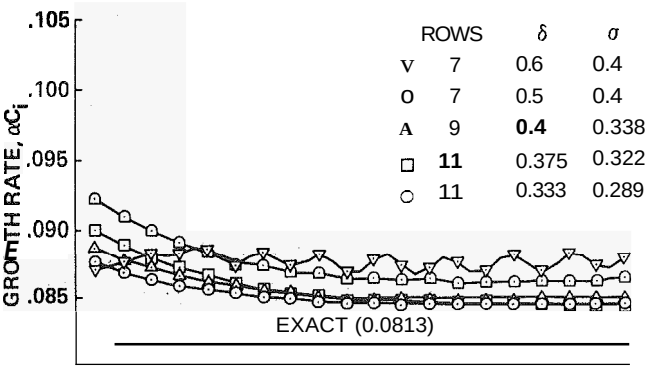

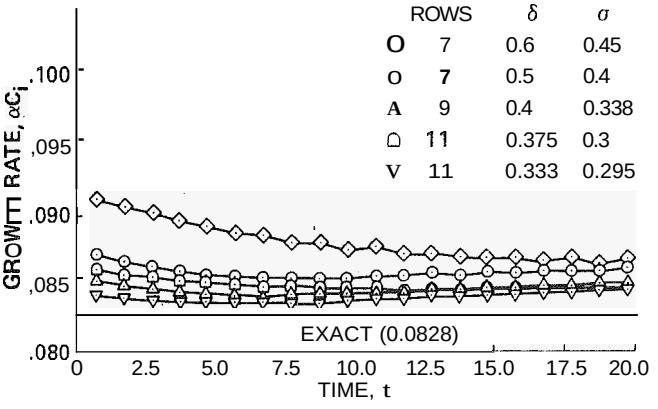

b) Error-function base flows

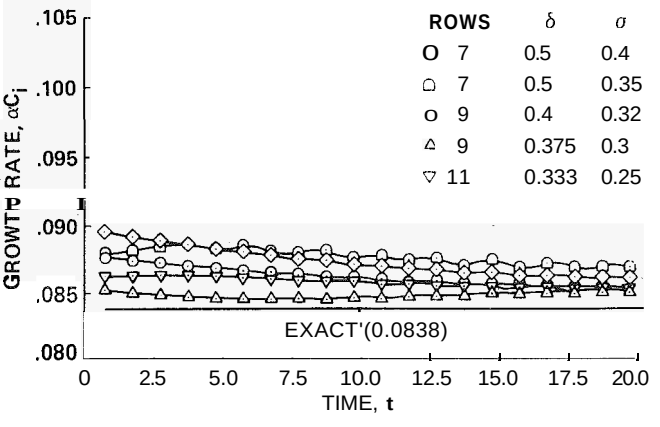

c) Polynomial base flows

Fig. 6 Growth rates calculated by vortex-blob method.

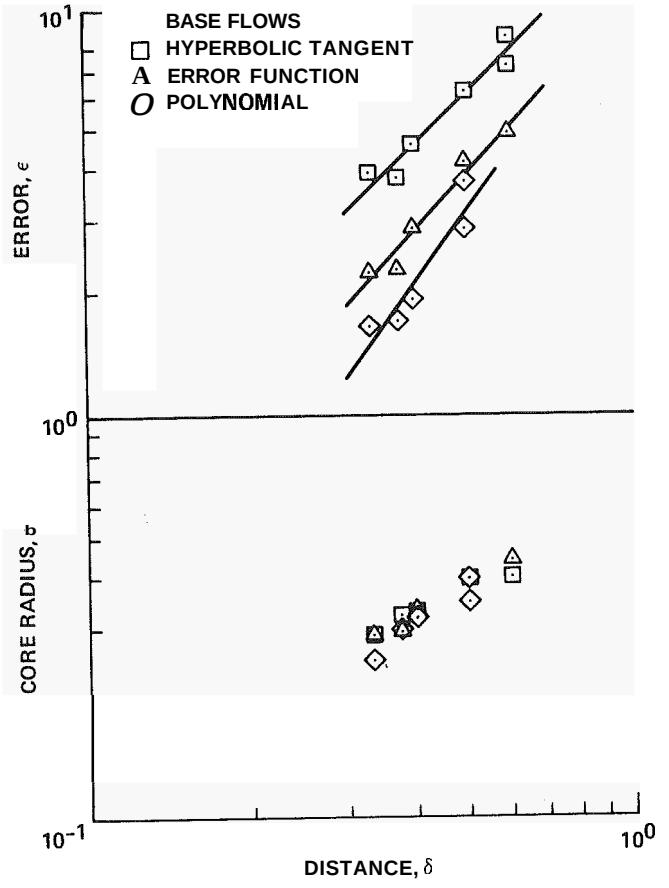

Fig. 7 Error and core radius versus vortex separation distance.

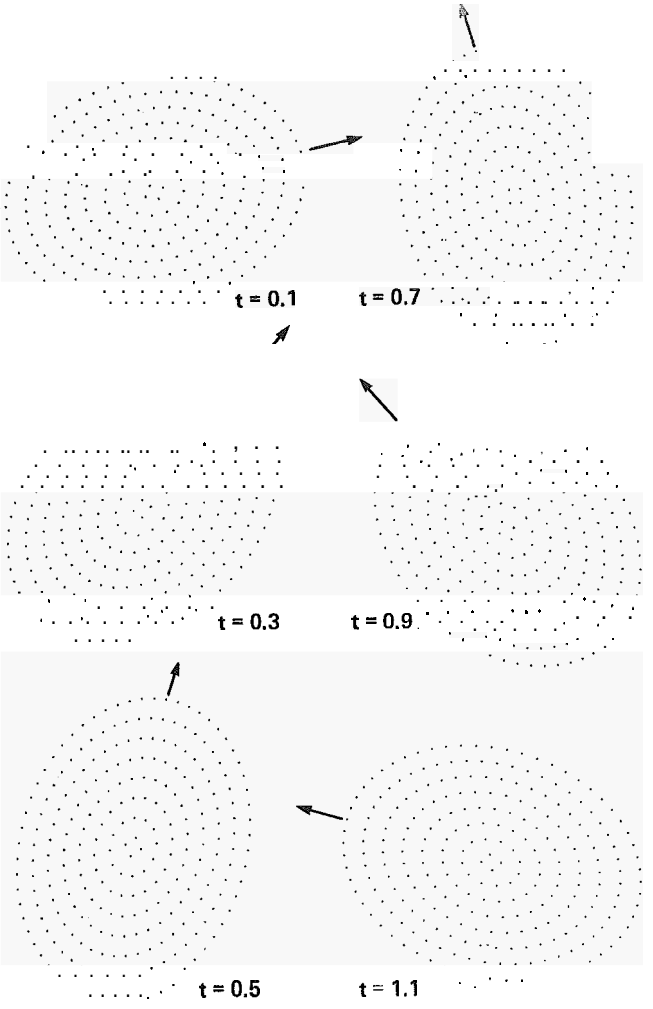

Fig. 8 Rotation of elliptic vortex without change of shape: $\sigma = 0.4$, eight rings, and scheme A (arror indicates major axis to facilitate observation of rotation).

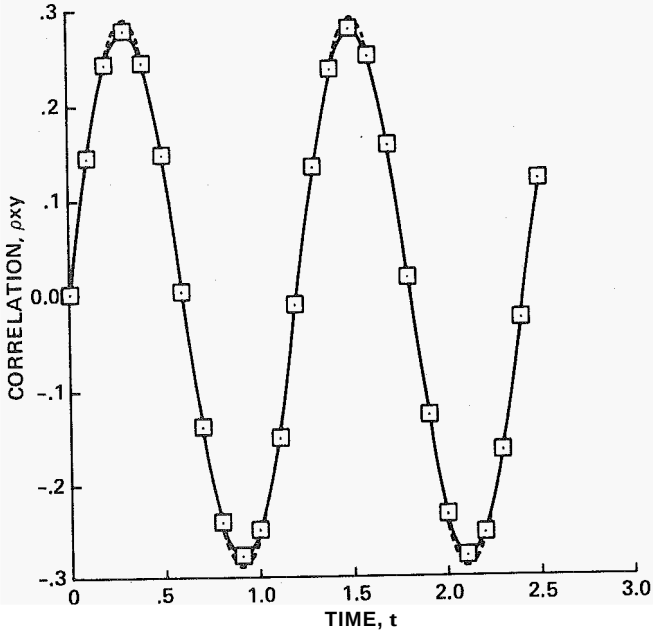

Fig. 9 Time history of ρ: (x,y) correlation of vortex–blob locations.

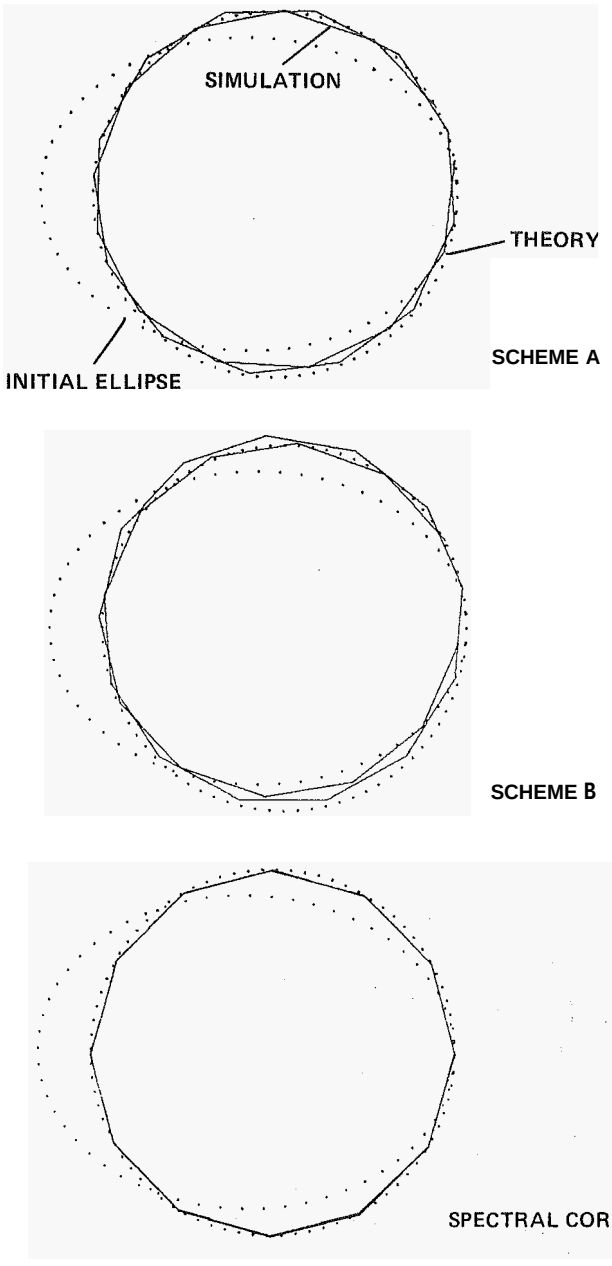

a) Particle paths

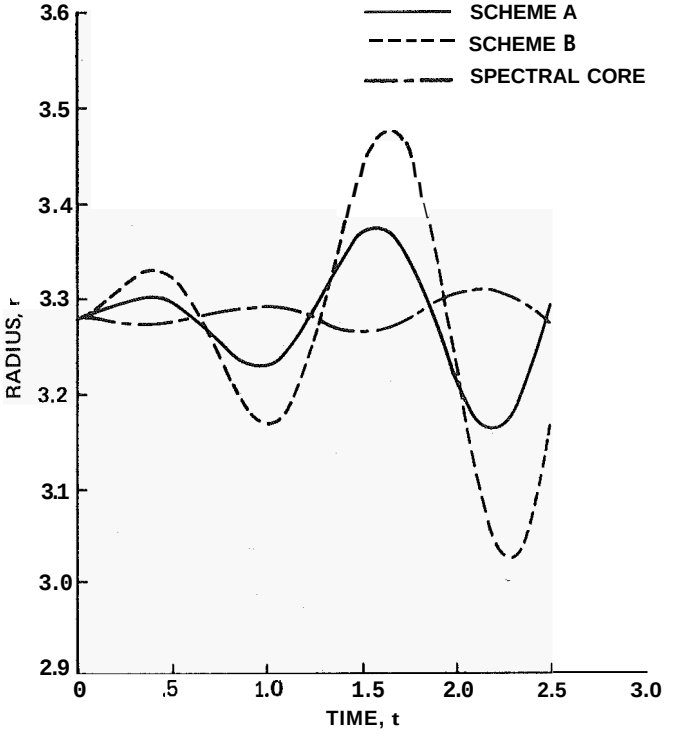

b) Time–history of radius from center of exact circle.

Fig. 10 A particle trajectory for three types.

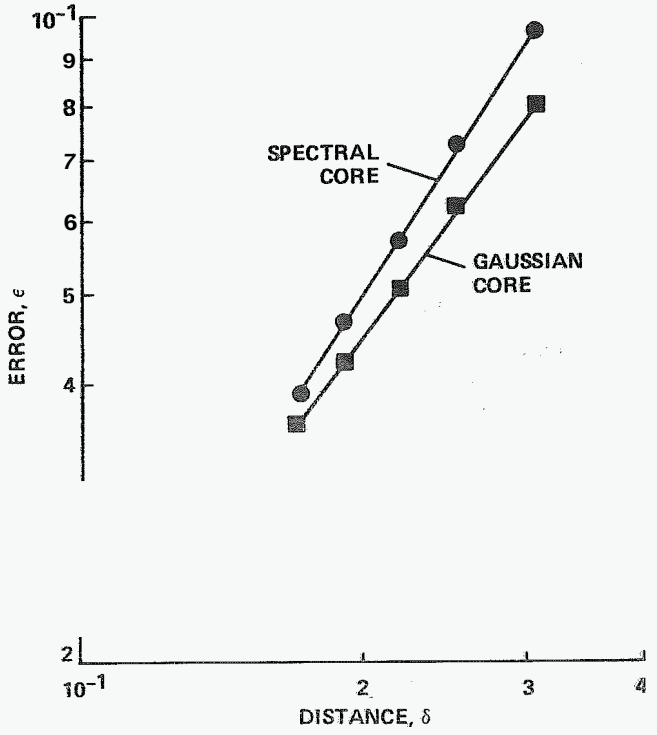

Fig. 11 Error in particle **(blob)** velocities at **initial tine** as **a** function of average distance between vortices.

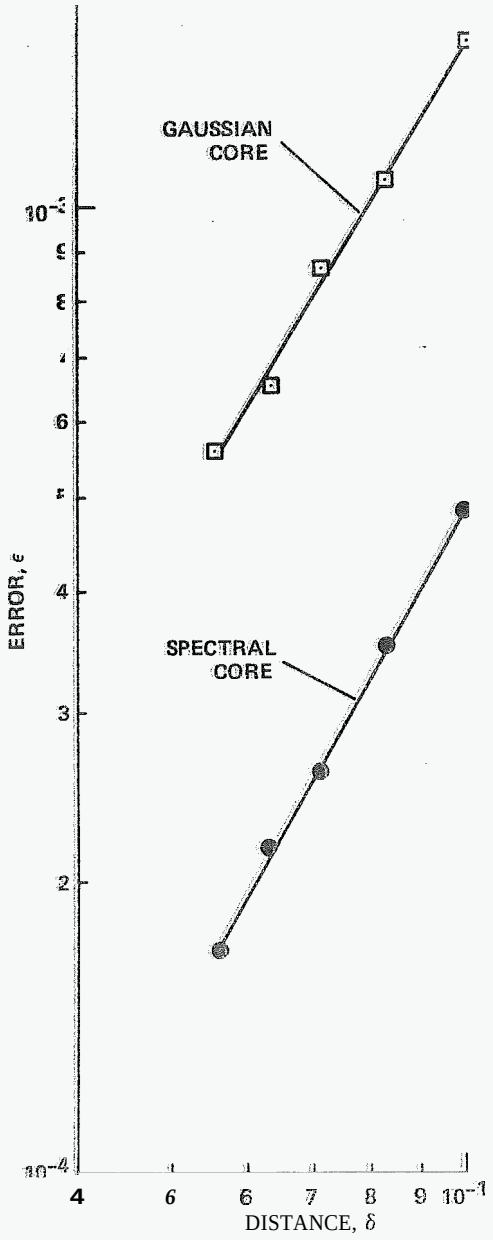

Fig. 12 Error in velocity field of circular vortex.

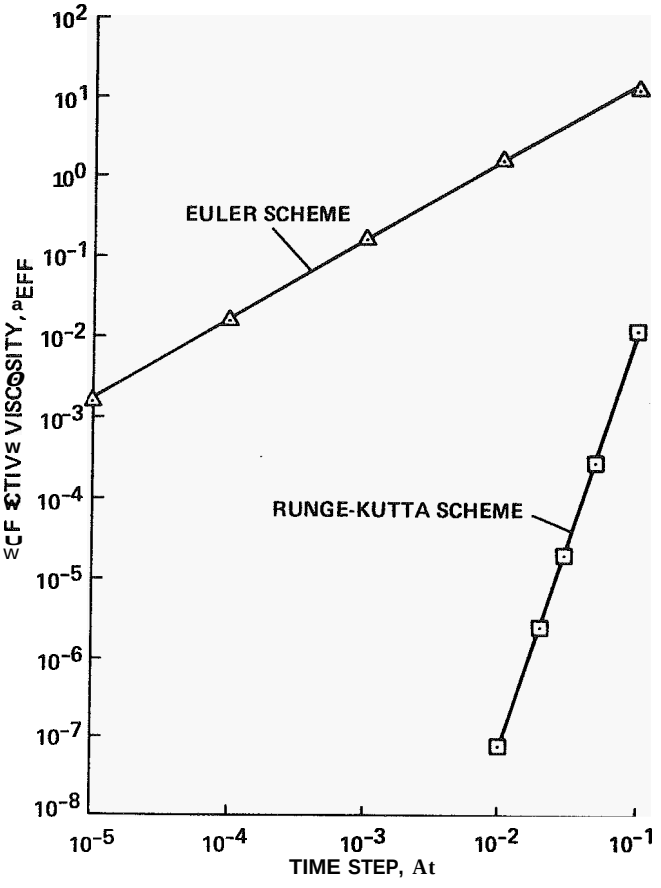

Fig. 13 Effect of time-step on effective viscosity in Euler and Runge-Kutta scheme: eight rings and $\sigma = 0.3$.